

## Light-scattering detection of quantum phases of ultracold atoms in optical lattices

Jinwu Ye,<sup>1,2</sup> J. M. Zhang,<sup>3</sup> W. M. Liu,<sup>3</sup> Keye Zhang,<sup>4</sup> Yan Li,<sup>4</sup> and Weiping Zhang<sup>4</sup>

<sup>1</sup>*Department of Physics, Capital Normal University, 100048 Beijing, China*

<sup>2</sup>*Department of Physics and Astronomy, Mississippi State University, P. O. Box 5167, Mississippi State, MS, 39762, USA*

<sup>3</sup>*Institute of Physics, Chinese Academy of Sciences, 100080 Beijing, China*

<sup>4</sup>*Department of Physics, East China Normal University, 200062 Shanghai, China*

(Received 2 June 2010; revised manuscript received 17 November 2010; published 16 May 2011)

Ultracold atoms loaded on optical lattices can provide unprecedented experimental systems for the quantum simulations and manipulations of many quantum phases. However, so far, how to detect these quantum phases effectively remains an outstanding challenge. Here, we show that the optical Bragg scattering of cold atoms loaded on optical lattices can be used to detect many quantum phases, which include not only the conventional superfluid and Mott insulating phases, but also other important phases, such as various kinds of charge density wave (CDW), valence bond solid (VBS), CDW supersolid (CDW-SS) and Valence bond supersolid (VB-SS).

DOI: [10.1103/PhysRevA.83.051604](https://doi.org/10.1103/PhysRevA.83.051604)

PACS number(s): 67.85.Hj, 03.75.-b, 42.50.-p

Various kinds of strongly correlated quantum phases of matter may have wide applications in quantum information processing, storage, and communications [1]. It was widely believed and also partially established that due to the tremendous tunability of all the parameters in this system, ultracold atoms loaded on optical lattices (OL) can provide unprecedented experimental systems for the quantum simulations and manipulations of these quantum phases and quantum phase transitions between these phases. For example, Mott and superfluid phases [2] may have been successfully simulated and manipulated by ultracold atoms loaded in a cubic optical lattice [3]. However, there are still at least two outstanding problems remaining. The first is how to realize many important quantum phases [1]. The second is that assuming the favorable conditions to realize these quantum phases are indeed achieved in experiments, how to detect them without ambiguity. In this Rapid Communication, we will focus on the second question. So far, the experimental way to detect these quantum phases is mainly through the time-of-flight (TOF) measurement [1,3], which simply opens the trap and turns off the optical lattice, lets the trapped atoms expand and interfere, and then takes the image. The atomic Bragg spectroscopy is based on stimulated matter waves scattering by *two* incident laser pulses [4,5] through the TOF measurements. The momentum [4] transfer Bragg spectroscopy was used to detect the Bogoliubov mode inside a Bose-Einstein condensate (BEC). The energy transfer [5] Bragg spectroscopy was used to detect the Mott gap in a Mott state in an optical lattice. Optical Bragg scattering [Fig. 1] has been used previously to study periodic lattice structures of cold atoms loaded on optical lattices [6]. It was also proposed as an effective method for the thermometry of fermions in an optical lattice [7] and to detect a putative antiferromagnetic (AF) ground state of fermions in an OL [8]. There are very recent optical Bragg scattering experimental data from a Mott state, a BEC, and an AF state [9]. The atomic Bragg spectroscopy and optical Bragg scattering are two different, but complementary, experimental methods.

In this Rapid Communication, we will develop a systematic theory of using the optical Bragg scattering [Fig. 1] to detect the nature of quantum phases of interacting bosons loaded in optical lattices. We show that the optical Bragg scattering

not only couples to the density order parameter but also to the *valence bond order* parameter due to the hopping of the bosons on the lattice. At integer fillings, when  $\vec{q}$  matches a reciprocal lattice vector  $\vec{K}$  of the underlying OL, there is an increase in the optical scattering cross section as the system evolves from the Mott to the SF state due to the increase of hopping in the SF state. At 1/2 filling, in the charge density wave (CDW) state, when  $\vec{q}$  matches the CDW ordering wave vector  $\vec{Q}_n$  and  $\vec{K}$ , there is a diffraction peak proportional to the CDW order parameter squared and the density squared, respectively [Fig. 3(a)]; the ratio of the two peaks is a good measure of the CDW order parameter. In the valence bond solid (VBS) state, when  $\vec{q}$  matches the VBS ordering wave vector  $\vec{Q}_K$ , there is a much smaller, but detectable diffraction peak proportional to the VBS order parameter squared; when it matches  $\vec{K}$ , there is also a diffraction peak proportional to the uniform density in the VBS state [Fig. 3(b)]. All the diffraction peaks scale as the square of the numbers of atoms inside the trap. All these characteristics can determine uniquely the CDW and VBS states at 1/2 filling and the corresponding CDW supersolid (CDW-SS) and Valence bond supersolid (VB-SS) slightly away from the 1/2 filling. In the following, we just take two-dimensional optical lattices as examples. The one-dimensional and three-dimensional cases can be similarly discussed.

The extended boson Hubbard model (EBHM) with various kinds of interactions, on all kinds of lattices and at different filling factors, is described by the following Hamiltonian [2,10–17]:

$$H_{\text{BH}} = -t \sum_{\langle ij \rangle} (b_i^\dagger b_j + \text{H.c.}) - \mu \sum_i n_i + \frac{U}{2} \sum_i n_i (n_i - 1) + V_1 \sum_{\langle ij \rangle} n_i n_j + V_2 \sum_{\langle ik \rangle} n_i n_k + \dots, \quad (1)$$

where  $n_i = b_i^\dagger b_i$  is the boson density;  $t$  is the nearest neighbor hopping which can be tuned by the depth of the optical lattice potential; the  $U$ ,  $V_1$ , and  $V_2$  are onsite; nearest neighbor (nn) and next nearest neighbor (nnn) interactions, respectively; and the  $\dots$  may include further neighbor interactions and possible ring-exchange interactions. The filling factor  $n = N_a/N$ , where  $N_a$  is the number of atoms, and  $N$  is the number

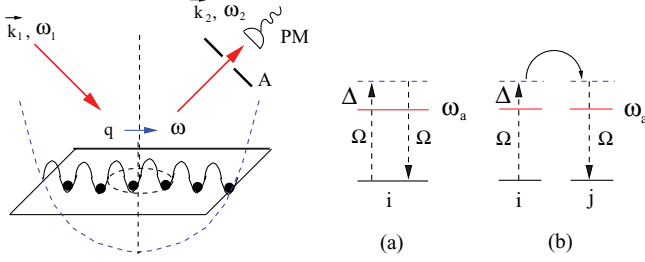


FIG. 1. (Color online) Optical Bragg scattering of cold atoms moving in two-dimensional optical lattices. The  $\vec{q} = \vec{k}_1 - \vec{k}_2$  and  $\omega = \omega_1 - \omega_2$  are momentum and energy transfers from the laser beams to the cold atoms, respectively. The A stands for an aperture, and the PM stands for a Photomultiplier. The offresonant scattering processes lead to (a) the onsite term and (b) the offsite term in Eq. (3).

of lattice sites. The onsite interaction  $U$  can be tuned by the Feshbach resonance [2]. Various kinds of optical lattices, such as honeycomb, triangular [18], body-centered-cubic [18], and Kagome lattices [19], can be realized by suitably choosing the geometry of the laser beams forming the optical lattices. There are many possible ways to generate longer range interactions  $V_1, V_2, \dots$  of ultracold atoms loaded in optical lattices. Being magnetically or electrically polarized, the  $^{52}\text{Cr}$  atoms [20] or polar molecules [21]  $^{40}\text{K} + ^{87}\text{Rb}$  (or  $^{39}\text{K} + ^{87}\text{Rb}$ ) interact with each other via long-range anisotropic dipole-dipole interactions. Loading the  $^{52}\text{Cr}$  or the polar molecules on a two-dimensional optical lattice with the dipole moments perpendicular to the trapping plane can be mapped to Eq. (1) with long-range repulsive interactions  $\sim p^2/r^3$ , where  $p$  is the dipole moment. The CDW supersolid phases studied by Quantum Monte Carlo (QMC) simulations [11] and described in [15] by the dual vortex method was numerically found to be stable in large parameter regimes in this system [22]. The generation of the ring exchange interaction has been discussed in [23]. Some of the important phases with long range interactions are listed in Fig. 2. Recently, the quantum entanglement properties of the VBS state were addressed in [24].

The interaction between the two laser beams in Fig. 1 with the two level bosonic atoms is:

$$H_{\text{int}} = \int d^2\vec{r} \Psi^\dagger(\vec{r}) \left\{ \frac{\vec{p}^2}{2m_a} + V_{\text{OL}}(\vec{r}) + \frac{\hbar\omega_a}{2} \sigma_z + \frac{\Omega}{2} \sum_l [e^{-i\omega_l t} \sigma^+ u_l(\vec{r}) + \text{H.c.}] \right\} \Psi(\vec{r}), \quad (2)$$

where  $\Psi(\vec{r}) = (\psi_e, \psi_g)$  is the two component boson annihilation operator, the incident and scattered lights in Fig. 1 have frequencies  $\omega_l$ , and mode functions  $u_l(\vec{r}) = e^{i\vec{k}_l \cdot \vec{r} + i\phi_l}$ . The Rabi frequencies  $\Omega$  are much weaker than the laser beams (not shown in Fig. 1), which form the optical lattices. When it is far off the resonance, the laser light-atom detunings  $\Delta_l = \omega_l - \omega_a$ , where  $\omega_a$  is the two level energy difference, are much larger than the Rabi frequency  $\Omega$  and the energy transfer  $\omega = \omega_1 - \omega_2$  [Figs. 1(a) and 1(b)], so  $\Delta_1 \sim \Delta_2 = \Delta$ . After adiabatically eliminating the upper level  $e$  of the two level atoms, expanding the ground-state atom field operator  $\psi_g(\vec{r}) = \sum_i b_i w(\vec{r} - \vec{r}_i)$  in Eq. (2), where  $w(\vec{r} - \vec{r}_i)$  is the localized

Wannier function of the lowest Bloch band corresponding to  $V_{\text{OL}}(\vec{r})$ , and  $b_i$  is the annihilation operator of an atom at the site  $i$  in the Eq. (1), then we get the effective interaction between the offresonant laser beams and the ground level  $g$ :

$$H_{\text{int}} = \hbar \frac{\Omega^2}{\Delta} e^{-i\omega t} \left( \sum_i^N J_{i,i} n_i + \sum_{\langle ij \rangle}^N J_{i,j} b_i^\dagger b_j \right), \quad (3)$$

where the interacting matrix element is  $J_{i,j} = \int d\vec{r} w(\vec{r} - \vec{r}_i) u_1^*(\vec{r}) u_2(\vec{r}) w(\vec{r} - \vec{r}_j) = J_{j,i}$ . The first term in Eq. (3) is the onsite term  $\hat{D} = \sum_i^N J_{i,i} n_i$  [Fig. 1(a)]. The second term is the offsite term [Fig. 1(b)]. Because the Wannier wave function  $w(\vec{r})$  can be taken as real in the lowest Bloch band, the offsite term can be written as  $\hat{K} = \sum_{\langle ij \rangle}^N J_{i,j} b_i^\dagger b_j = \sum_{\langle ij \rangle}^N J_{i,j} (b_i^\dagger b_j + \text{H.c.})$ , which is nothing but the offsite coupling to the nearest neighbor kinetic energy of the bosons  $K_{ij} = b_i^\dagger b_j + \text{H.c.}$

It is easy to show that

$$\hat{D}(\vec{q}) = f_0(\vec{q}) \sum_{i=1}^N e^{-i\vec{q} \cdot \vec{r}_i} n_i = N f_0(\vec{q}) n(\vec{q}), \quad (4)$$

where  $\vec{q} = \vec{k}_1 - \vec{k}_2$ ,  $f_0(\vec{q}) = \int d\vec{r} e^{-i\vec{q} \cdot \vec{r}} w^2(\vec{r})$ , and  $n(\vec{q}) = \frac{1}{N} \sum_{i=1}^N e^{-i\vec{q} \cdot \vec{r}_i} n_i = \sum_{\vec{k}} b_{\vec{k}}^\dagger b_{\vec{k}+\vec{q}}$  is the Fourier transform of the density operator at the momentum  $\vec{q}$ . Note that  $n(\vec{q}) = n(\vec{q} + \vec{K})$  where the  $\vec{K}$  is a reciprocal lattice vector. The wave vector is confined to  $L^{-1} < q < a^{-1}$ , where the trap size  $L \sim 100 \mu\text{m}$ , and the lattice constant  $a \sim 0.5 \mu\text{m}$  in Fig. 1. In fact, more information is encoded in the offsite kinetic coupling in Eq. (3). In a square lattice, since the bonds are either oriented along the  $\hat{x}$  axis,  $\vec{r}_j - \vec{r}_i = \hat{x}$ , or along the  $\hat{y}$  axis,  $\vec{r}_j - \vec{r}_i = \hat{y}$ , we have

$$\hat{K}_{\square} = N [f_x(\vec{q}) K_x(\vec{q}) + f_y(\vec{q}) K_y(\vec{q})], \quad (5)$$

where  $K_\alpha(\vec{q}) = \frac{1}{N} \sum_{i=1}^N e^{-i\vec{q} \cdot \vec{r}_i} K_{i,i+\alpha} = e^{i\vec{q} \cdot \vec{a}/2} \sum_{\vec{k}} \cos k_\alpha b_{\vec{k}}^\dagger b_{\vec{k}+\vec{q}}$ ,  $\alpha = x, y$  are the Fourier transforms of the kinetic energy operator  $K_{ij} = b_i^\dagger b_j + \text{H.c.}$  along  $\alpha = x, y$  bonds at the momentum  $\vec{q}$  and the “form” factors  $f_\alpha(\vec{q}) = f(\vec{q}, \vec{r}_i - \vec{r}_j = \alpha) = \int d\vec{r} e^{-i\vec{q} \cdot \vec{r}} w(\vec{r}) w(\vec{r} + \vec{r}_i - \vec{r}_j)$ . Note that  $K_\alpha(\vec{q}) = K_\alpha(\vec{q} + \vec{K})$ . Following the harmonic approximation used in [2], we can estimate that  $f_0(\pi, 0) \sim \exp[-\frac{1}{4}(V_0/E_r)^{-1/2}]$ ,  $f_x(\pi, 0) \sim i \exp[-\frac{1}{4}(V_0/E_r)^{-1/2} - \frac{\pi^2}{4}(V_0/E_r)^{1/2}]$ , so  $|f_x(\pi, 0)/f_0(\pi, 0)| \sim \exp(-\frac{\pi^2}{4} \sqrt{V_0/E_r})$ , where  $V_0$  and  $E_r = \hbar^2 k^2/2m$  are the strength of the optical lattice potential and the recoil energy, respectively [2]. The  $f_0(\pi, 0)$  is close to 1, when  $V_0/E_r > 4$ . It is instructive to relate this ratio to that of the hopping  $t$  over the onsite interaction  $U$  in the Eq. (1):  $|f_x(\pi, 0)/f_0(\pi, 0)| \sim \frac{t}{U} \frac{a_s}{a}$ , where  $a_s$  is the zero field scattering length and  $a = \lambda/2 = \pi/k$  is the OL constant; using the typical values  $t/U \sim 10^{-1}$  and  $a_s/a \sim 10^{-2}$ , one can estimate  $|f_\alpha/f_0| \sim 10^{-3}$ . Note that the harmonic approximation works well only in a very deep optical lattice  $V_0 \gg E_r$ , so the above value *underestimates* the ratio, so we expect  $|f_\alpha/f_0| \geq 10^{-3}$ .

The differential scattering cross section of the light from the cold atom systems in the Fig. 1 can be calculated by using

the standard linear response theory:

$$\frac{d\sigma}{d\Omega dE} = \mathcal{S}(\vec{q}, \omega) \sim \left(\frac{\Omega^2}{\Delta}\right)^2 N^2 \times \left[ |f_0(\vec{q})|^2 S_n(\vec{q}, \omega) + \sum_{\alpha=\hat{x}, \hat{y}} |f_\alpha(\vec{q})|^2 S_{K_\alpha}(\vec{q}, \omega) \right], \quad (6)$$

where  $\vec{q} = \vec{k}_1 - \vec{k}_0$ ,  $\omega = \omega_1 - \omega_2$ , and the  $S_n(\vec{q}, \omega) = \langle n(-\vec{q}, -\omega)n(\vec{q}, \omega) \rangle$  is the dynamic density-density response function, whose Lehmann representation was listed in [4]. The  $S_{K_\alpha}(\vec{q}, \omega) = \langle K_\alpha(-\vec{q}, -\omega)K_\alpha(\vec{q}, \omega) \rangle$  is the bond-bond response function, whose Lehmann representation can be obtained from that of the  $S_n(\vec{q}, \omega)$  simply by replacing the density operator  $n(\vec{q})$  by the bond operator  $K_\alpha(\vec{q})$ . The integrated scattering cross section over the final energy  $\frac{d\sigma}{d\Omega} = \int dE \frac{d\sigma}{d\Omega dE}$  is proportional to the *equal-time* response function  $\frac{d\sigma}{d\Omega} = \mathcal{S}(\vec{q}) \sim \left(\frac{\Omega^2}{\Delta}\right)^2 N^2 [|f_0(\vec{q})|^2 S_n(\vec{q}) + \sum_{\alpha=\hat{x}, \hat{y}} |f_\alpha(\vec{q})|^2 S_{K_\alpha}(\vec{q})]$ .

We first look at the superfluid to Mott transition at the integer filling factor  $n$ . When  $\vec{q}$  is equal to the shortest reciprocal lattice vector  $\vec{K} = (2\pi, 0)$ ; in the Mott state,  $\frac{d\sigma^M}{d\Omega} \sim |f_0^M(2\pi, 0)|^2 N^2 n^2$ ; in the superfluid state,  $\frac{d\sigma^{SF}}{d\Omega} \sim |f_0^{SF}(2\pi, 0)|^2 N^2 n^2 + 2|f_x^{SF}(2\pi, 0)|^2 N^2 B^2$ , where  $B$  is the average kinetic energy on a bond in the superfluid side. Because  $|f_0^{SF}(2\pi, 0)|^2 \sim |f_0^M(2\pi, 0)|^2 \sim 1$ , and  $B$  is appreciable only in the superfluid side, we expect a dramatic increase of the scattering cross section

$$\frac{d\sigma^{SF}}{d\Omega} - \frac{d\sigma^M}{d\Omega} = 2|f_x^{SF}(2\pi, 0)|^2 N^2 B^2 \quad (7)$$

across the Mott to the SF transition due to the prefactor  $N^2$ . This prediction could be tested immediately. Surprisingly, there is no such optical Bragg scattering experiment in the superfluid yet.

In the CDW with  $\vec{Q}_n = (\pi, \pi)$  in Fig. 2(a), due to the lack of VBS order, the second term in Eq. (6) can be neglected, so that

$$\frac{d\sigma}{d\Omega dE} \Big|_{\text{CDW}} \sim \left(\frac{\Omega^2}{\Delta}\right)^2 N^2 |f_0(\vec{q})|^2 S_n(\vec{q}, \omega), \quad (8)$$

which should show a peak at  $\vec{q} = \vec{Q}_n$  [Fig. 3(a)], whose amplitude scales as the *square* of the number of atoms inside the trap  $\sim |f_0(\pi, \pi)|^2 N^2 m^2$ , where  $m = n_A - n_B$  is the CDW order parameter [15]. When  $\vec{q} = \vec{K}$ , then

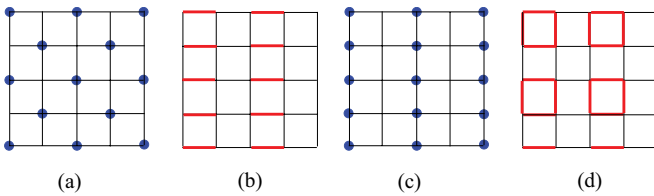


FIG. 2. (Color online) (a) CDW phase in a square lattice at  $n_0 = 1/2$  with ordering wave vector  $\vec{Q}_n = (\pi, \pi)$ . (b) Valence bond solid (VBS) phases with ordering wave vector  $\vec{Q}_K = (\pi, 0)$ , where the kinetic energy  $\langle K_{ij} \rangle = \langle b_i b_j + \text{H.c.} \rangle$  takes a nonzero constant  $K$  in the two sites connected with a dimer, but takes 0 in the two sites without a dimer. (c) Stripe CDW order at  $\vec{Q}_n = (\pi, 0)$  and (d) plaquette VBS order at  $\vec{Q}_K = (\pi, 0), (0, \pi)$  [2,10–17].

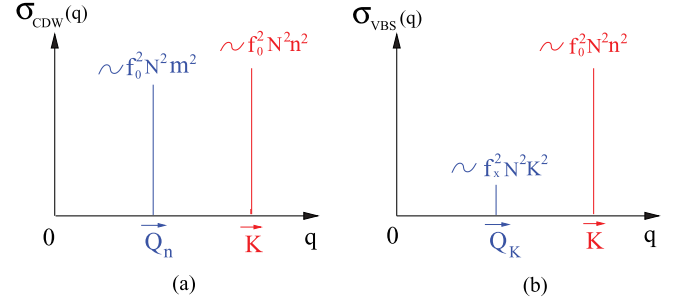


FIG. 3. (Color online) Optical scattering cross section in (a) CDW, where the ratio of the peak at  $\vec{Q}_n$  over that at  $\vec{K}$  is  $\sim m^2/n^2 \sim 1$ , and (b) VBS state, where the ratio of the peak at  $\vec{Q}_K$  over that at  $\vec{K}$  is  $\sim |f_x/f_0|^2 K^2/n^2 \geq 10^{-5}$ , which still should be visible in the current optical Bragg scattering experiments.

$\mathcal{S}_{\text{CDW}}(\vec{K}) \sim |f_0(2\pi, 0)|^2 N^2 n^2$ , where  $f_0(2\pi, 0) \sim f_0^2(\pi, \pi)$  [Fig. 3(a)]. So the ratio of the two peaks in Fig. 3(a) is  $\sim m^2/n^2$  if one neglects the very small difference of the two form factors. Slightly away from  $1/2$  filling, the CDW in Fig. 2(a) may turn into a CDW-SS [25] phase through a second order phase transition [15]. Then, we have  $\langle n(\vec{q}) \rangle = m\delta_{\vec{q}, \vec{Q}_n} + n\delta_{\vec{q}, 0}$  where  $n = n_A + n_B = 1/2 + \delta n$ . The superfluid density  $\rho_s \sim \delta n = n - 1/2$ . The scattering cross section inside the CDW-SS:  $\mathcal{S}_{\text{CDW-SS}}(\vec{Q}_n) \sim |f_0(\pi, \pi)|^2 N^2 m^2$  stays more or less the same as that inside the CDW, but  $\mathcal{S}_{\text{CDW-SS}}(\vec{K}) \sim |f_0(2\pi, 0)|^2 N^2 n^2 + 2|f_x(2\pi, 0)|^2 N^2 (\delta n)^2 B^2$  will increase. The  $B$  is the average bond strength due to very small superfluid component  $\rho_s \sim \delta n = n - 1/2$  flowing through the whole lattice. So the right peak in Fig. 3(a) will increase due to the increase of the total density and the superfluid component inside the CDW-SS phase.

Now we discuss the VBS state with  $\vec{Q}_K = (\pi, 0)$  in Fig. 2(b). Due to the *uniform* distribution of the density in the VBS, when  $\vec{q} = \vec{K}$ , the second term in Eq. (6) can be neglected, so there is a diffraction peak [Fig. 3(b)] whose amplitude scales as the *square* of the number of atoms inside the trap  $\sim |f_0(2\pi, 0)|^2 N^2 n^2$ , where  $f_0(2\pi, 0) \sim f_0^4(\pi, 0)$  and  $n = 1/2$  is the uniform density in the VBS state. However, when one tunes  $\vec{q}$  near  $\vec{Q}_K$ , the first term in Eq. (6) can be neglected; then,

$$\frac{d\sigma}{d\Omega dE} \Big|_{\text{VBS}} \sim \left(\frac{\Omega^2}{\Delta}\right)^2 N^2 \sum_{\alpha=\hat{x}, \hat{y}} |f_\alpha(\vec{q})|^2 S_{K_\alpha}(\vec{q}, \omega), \quad (9)$$

which should show a peak at  $\vec{q} = \vec{Q}_K$  signifying the VBS ordering at  $\vec{Q}_K$ , whose amplitude scales also as the *square* of the number of atoms inside the trap  $\sim |f_x(\pi, 0)|^2 N^2 K^2$ , where  $K = K_x - K_y$  is the VBS order parameter [15]. So the ratio of the VBS peak at  $\vec{q} = \vec{Q}_K$  over the uniform density peak at  $\vec{q} = \vec{K}$  is  $\sim [K^2/n^2] |f_x(\pi, 0)/f_0(2\pi, 0)|^2 \geq 10^{-5}$  in Fig. 3(b). Note that the smallness of  $|f_x|^2$  is compensated by the large number of atoms  $N \sim 10^6$ ,  $|f_x|^2 N^2 = (|f_x|^2 N) \times N \sim N \sim 10^6$ . Therefore, the Bragg scattering cross section from the VBS order is  $\geq 10^{-5}$  smaller than that at  $\vec{q} = \vec{K}$  at the same incident energy  $I_{\text{in}}$  [Fig. 3(b)], but still  $\sim 10^6$  above the background, so very much visible in the current optical Bragg scattering experiments. Slightly away from  $1/2$  filling, the VBS may

turn into a VB Supersolid (VB-SS) through a second-order transition [15]. We have  $\langle K_x(\vec{q}) \rangle = B\delta_{\vec{q},0} + K\delta_{\vec{q},\vec{Q}_K}$  and  $\langle n(\vec{q}) \rangle = (\delta n + 1/2)\delta_{\vec{q},0}$ . The superfluid density  $\rho_s \sim \delta n = n - 1/2$ . The scattering cross section inside VB-SS:  $S_{\text{VB-SS}}(\vec{Q}_K) \sim |f_x(\pi,0)|^2 N^2 K^2$  stays more or less the same as that inside the VBS, but  $S_{\text{VB-SS}}(\vec{K}) \sim |f_0(2\pi,0)|^2 N^2 n^2 + |f_x(2\pi,0)|^2 N^2 (\delta n)^2 B_x^2 + |f_y(2\pi,0)|^2 N^2 (\delta n)^2 B_y^2$ , where  $n = 1/2 + \delta n$  and the  $B_x, B_y$  are the average bond strengths along  $x$  and  $y$ , respectively, due to a very small superfluid component  $\rho_s \sim \delta n = n - 1/2$  flowing through the whole lattice. So the right peak in Fig. 3(b) will increase due to the increase of the total density and the superfluid component inside the VB-SS phase. Very similarly, one can discuss the VBS order at  $\vec{q} = \vec{Q}_K = (0,\pi)$ . For the plaquette VBS order in Fig. 2(d), then one should be able to see the  $S_K(\vec{q})$  peaks at both  $(\pi,0)$  and  $(0,\pi)$ . So the dimer VBS and the plaquette VBS can also be distinguished by the optical Bragg scattering.

In this Rapid Communication, we only focused on the optical Bragg scattering detections of the various ground states in a square lattice. The detections of the excitation spectra, the generalization to frustrated lattices, the effects of finite temperature and a harmonic trap will be discussed in a future publication [26].

We thank A. V. Balatsky, G. G. Batrouni, Jason Ho, R. Hulet, S. V. Isakov, Juan Pino, and Han Pu for helpful discussions. J. Ye's research is supported by NSF-DMR-0966413, NSFC-11074173 is supported at KITP in part by the NSF under Grant No. PHY-0551164, and is supported at KITP-C by the Project of Knowledge Innovation Program (PKIP) of the Chinese Academy of Sciences. W. M. Liu's research was supported by NSFC-10874235. W. P. Zhang's research was supported by the National Basic Research Program of China (973 Program) under Grant No. 2011CB921604, and NSFC under Grants No. 10588402 and 10474055.

- 
- [1] For a review, see M. Lewenstein *et al.*, *Adv. Phys.* **56**, 243 (2007); I. Bloch, J. Dalibard, and W. Zwerger, *Rev. Mod. Phys.* **80**, 885 (2008).
- [2] D. Jaksch, C. Bruder, J. I. Cirac, C. W. Gardiner, and P. Zoller, *Phys. Rev. Lett.* **81**, 3108 (1998).
- [3] M. Greiner *et al.*, *Nature (London)* **415**, 39 (2002).
- [4] M. Kozuma *et al.*, *Phys. Rev. Lett.* **82**, 871 (1999); J. Stenger *et al.*, *ibid.* **82**, 4569 (1999); D. M. Stamper-Kurn *et al.*, *ibid.* **83**, 2876 (1999); J. Steinhauer, R. Ozeri, N. Katz, and N. Davidson, *ibid.* **88**, 120407 (2002); S. B. Papp *et al.*, *ibid.* **101**, 135301 (2008); P. T. Ernst *et al.*, *Nature Phys.* **6**, 56 (2010).
- [5] T. Stoferle, H. Moritz, C. Schori, M. Kohl, and T. Esslinger, *Phys. Rev. Lett.* **92**, 130403 (2004).
- [6] G. Birkl, M. Gatzke, I. H. Deutsch, S. I. Rolston, and W. D. Phillips, *Phys. Rev. Lett.* **75**, 2823 (1995); M. Weidemuller, A. Hemmerich, A. Gorlitz, T. Esslinger, and T. W. Hansch, *ibid.* **75**, 4583 (1995); M. Weidemuller, A. Gorlitz, T. W. Hansch, and A. Hemmerich, *Phys. Rev. A* **58**, 4647 (1998).
- [7] J. Ruostekoski, C. J. Foot, and A. B. Deb, *Phys. Rev. Lett.* **103**, 170404 (2009).
- [8] T. A. Corcovilos, S. K. Baur, J. M. Hitchcock, E. J. Mueller, and R. G. Hulet, *Phys. Rev. A* **81**, 013415 (2010).
- [9] I. Bloch (private communication).
- [10] G. Murthy, D. Arovas, and A. Auerbach, *Phys. Rev. B* **55**, 3104 (1997).
- [11] F. Hebert *et al.*, *Phys. Rev. B* **65**, 014513 (2001); P. Sengupta, L. P. Pryadko, F. Alet, M. Troyer, and G. Schmid, *Phys. Rev. Lett.* **94**, 207202 (2005).
- [12] S. V. Isakov, S. Wessel, R. G. Melko, K. Sengupta, and Y. B. Kim, *Phys. Rev. Lett.* **97**, 147202 (2006); K. Damle and T. Senthil, *ibid.* **97**, 067202 (2006).
- [13] L. Balents, L. Bartosch, A. Burkov, S. Sachdev, and K. Sengupta, *Phys. Rev. B* **71**, 144508 (2005).
- [14] L. Jiang and J. Ye, *J. Phys. Condens. Matter* **18**, 6907 (2006).
- [15] J. Ye, *Nucl. Phys. B* **805**, 418 (2008).
- [16] Y. Chen and J. Ye, e-print arXiv:0804.3429v3 [cond-mat], e-print arXiv:cond-mat/0612009v4.
- [17] J. Y. Gan *et al.*, *Phys. Rev. B* **75**, 214509 (2007).
- [18] G. Grynberg, B. Lounis, P. Verkerk, J. Y. Courtois, and C. Salomon, *Phys. Rev. Lett.* **70**, 2249 (1993).
- [19] L. Santos *et al.*, *Phys. Rev. Lett.* **93**, 030601 (2004); B. Damski *et al.*, *Phys. Rev. A* **72**, 053612 (2005).
- [20] A. Griesmaier, J. Werner, S. Hensler, J. Stuhler, and T. Pfau, *Phys. Rev. Lett.* **94**, 160401 (2005).
- [21] K.-K. Ni *et al.*, *Science* **322**, 231 (2008).
- [22] B. Capogrosso-Sansone, C. Trefzger, M. Lewenstein, P. Zoller, and G. Pupillo, *Phys. Rev. Lett.* **104**, 125301 (2010).
- [23] H. P. Büchler, M. Hermele, S. D. Huber, M. P. A. Fisher, and P. Zoller, *Phys. Rev. Lett.* **95**, 040402 (2005).
- [24] A. Chandran, D. Kaszlikowski, A. SenDe, U. Sen, and V. Vedral, *Phys. Rev. Lett.* **99**, 170502 (2007).
- [25] For a supersolid in a continuous system (namely without an underlying OL), see J. Ye, *Phys. Rev. Lett.* **97**, 125302 (2006); *Europhys. Lett.* **82**, 16001 (2008); *J. Low Temp. Phys.* **160**, 71 (2010).
- [26] J. Ye *et al.*, e-print arXiv:0812.4077v4 [cond-mat].